The structural and electrical evolution of graphene by oxygen plasma-induced disorder

2009 Nanotechnology 20 375703

(http://iopscience.iop.org/0957-4484/20/37/375703)

Nanotechnology **20** (2009) 375703 (8pp) doi:10.1088/0957-4484/20/37/375703

The structural and electrical evolution of graphene by oxygen plasma-induced disorder

Dong Chul Kim, Dae-Young Jeon, Hyun-Jong Chung, YunSung Woo, Jai Kwang Shin and Sunae Seo

Samsung Advanced Institute of Technology, Samsung Electronics Company Ltd, Suwon 440-600, Korea

E-mail: sunaeseo@samsung.com

Received 10 June 2009, in final form 29 July 2009
Published 26 August 2009
Online at stacks.iop.org/Nano/20/375703

Abstract

Evolution of a single graphene layer with disorder generated by remote oxygen plasma irradiation is investigated using atomic force microscopy, Raman spectroscopy and electrical measurement. Gradual changes of surface morphology from planar graphene to isolated granular structure associated with a decrease of transconductance are accounted for by two-dimensional percolative conduction by disorder and the oxygen plasma-induced doping effect. The corresponding evolution of Raman spectra of graphene shows several peculiarities such as a sudden appearance of a saturated D peak followed by a linear decrease in its intensity, a relatively inert characteristic of a D′ peak and a monotonic increase of a G peak position as the exposure time to oxygen plasma increases. These are discussed in terms of a disorder-induced change of Raman spectra in the graphite system.

(Some figures in this article are in colour only in the electronic version)

1. Introduction

Since the first report on graphene and its electric field effect, there has been a great deal of interest in this two-dimensional honeycombed carbon structure due to its unique electronic properties [1–6]. One merit of graphene is that devices of different designs can be easily fabricated by using conventional lithographic patterning and etching processes. In the fabrication of graphene devices such as nanoribbon or nanodot transistors, the etching process of graphene itself is very critical since the etching-induced disorder at graphene edges affects the electrical transport dramatically [7–10]. Understanding and controlling the detailed etching mechanism of graphene is necessary for fabricating and analysing graphene devices. Up to now the direct oxygen plasma etching method has been generally used for the patterning and etching of graphene. The oxygen plasma is generated by biasing the sample loading plate and the sample is directly immersed in the plasma glow discharge. Multiple graphene layers are sufficiently etched away in less than a few seconds [11]. In this method, the etching rate of graphene is too fast, making it almost impossible to control the etching deliberately and thus investigate the detailed etching processes of a single graphene layer.

In this paper, a remote oxygen (R-O_2) plasma method using a downstream inductively coupled plasma asher is applied to a single graphene layer. The oxygen plasma is not directly coupled to the sample loading plate and arrives at the sample surface solely by diffusion, giving a gentle oxygen plasma treatment to the sample. By adjusting the plasma conditions, the etching time of a single graphene layer can be extended to more than a few minutes. This enables us to study the detailed changes of graphene during exposure to oxygen plasma. It is naturally expected that the application of oxygen plasma to graphene would introduce structural defects and disorder. It is also interesting to investigate the disorder effect on a single graphene layer in connection to previous research on graphite with disorder [12, 13].

2. Experimental procedure

A single graphene layer sample was prepared by mechanical exfoliation of Kish graphite (Toshiba Ceramics.) onto 300 nm

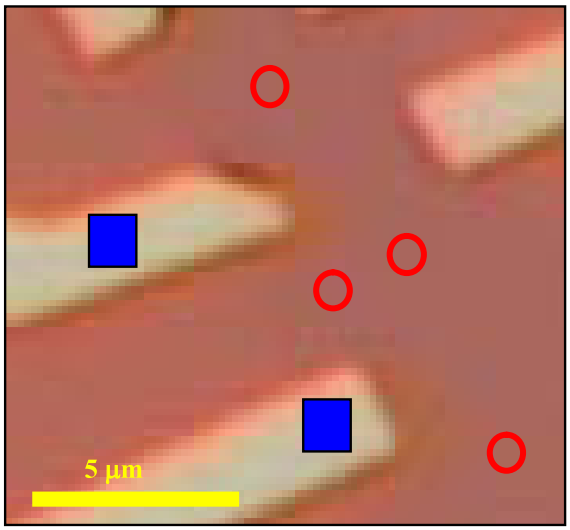

Figure 1. Optical microscope image (500×) of the measured sample. The red circles denote the spots where the Raman spectra were collected. Blue squares denote two-probe electrodes where the source–drain voltage is applied.

thick SiO_2 thermally grown on a p-doped Si substrate [3]. After identifying a single graphene layer with an optical microscope and Raman spectroscopy, the electrode patterning was carried out. E-beam lithography with PMMA e-beam resist was used to define the lead patterns on the graphene. Cr (5 nm)/Au (45 nm) were deposited using an e-beam evaporator for lead patterns. After the fabrication of lead patterns, the electrode patterns which connect the lead patterns to the electrodes for measurement were fabricated by using photolithography with AZ5214 photoresist. Cr (5 nm)/Au (100 nm) were subsequently deposited for electrode patterns (figure 1).

The oxygen plasma treatment was carried out using a remote oxygen (R-O_2) plasma method using a downstream inductively coupled plasma asher (DFS-200, BMR Technology Corp.). Operational conditions of 900 W radio-frequency power for remote plasma generation and 300 mTorr for oxygen pressure usually resulted in a complete etching time of more than 3 min for a single graphene layer. After carrying out each timestep of oxygen plasma treatment on the graphene sample, atomic force microscopy (AFM), Raman spectroscopy and electrical measurements were used to characterize the structural and electrical changes.

AFM images were measured in air using the tapping mode in an SPA 500 (Seiko Instruments Inc.) with SI-DF40 tips having a radius of curvature $\leqslant$15 nm. Raman measurements were performed in air using a 514.5 nm wavelength Ar laser (Renishaw micro-Raman measurement system). The spot diameter was $\sim$2 μm with a 50× objective lens. The power intensity of the incident laser was always checked and kept at $\sim$0.9 mW. The Raman spectra of the sample were collected from the same spots as denoted by red circles in figure 1(b) after carrying out each timestep of the oxygen plasma treatment. Reproducibility of the Raman spectra was checked by measuring the same spot several times at random time intervals, in which case no spectral changes were observed.

The electrical measurement was carried out in a two-probe configuration with the gate voltage applied to the back gate using a semiconductor characterization system (Keithley SCS 4200) in a vacuum probe station. A vacuum level of $<10^{-5}$ mTorr was maintained during the measurements at room temperature.

3. Results and discussion

Figure 2 shows the evolution of AFM images of a single graphene layer with an increase of the exposure time (t) to R-O_2 plasma. It should be noted that all AFM images were taken at the same spot of the sample after each R-O_2 plasma treatment. The height profiles of selected AFM images are shown in figure 3. In the pristine graphene sample before any exposure to the R-O_2 plasma the measured thickness (t_H) and the root-mean-square surface roughness (t_{RMS}) are 0.9–1.2 nm and 0.32 nm, respectively (figures 2(a) and 3). However, after just 5 s exposure to the R-O_2 plasma, the surface morphology is drastically changed to crumpled with a sharp increase of t_{RMS} to 1.04 nm. The increase is mainly due to the random appearance of 'white' spots (sizes up to $\sim$100 nm in diameter and 4–6 nm in height) throughout the surface (figure 2(b)). The origin of this is not clear. After exposing the sample for 35 s, the 'white' spots mostly disappear. The crumpled surface structure appears to be composed of randomly oriented cigar-type clusters ($\sim$100 nm in overall length and $\sim$50 nm in width) surrounded by valleys with a depth of 1–1.5 nm (see the inset in figure 2(c)). Although t_{RMS} decreases down to 0.39 nm, close to that of the pristine sample, the overall t_H increases up to $\sim$2.5 nm with a peak-to-valley height up to $\sim$1.5 nm (figure 3). Re-deposition or conglomeration of chemical residues or graphitic carbons occurring during the plasma treatment might be a possible cause for the observed increase in thickness [14]. Another possibility would be the chemical functionalization by oxygen plasma. It was reported that, for a graphene oxide sheet, the relative increase of thickness by bearing oxygen-containing groups on both surfaces would be about 0.2–0.5 nm [15]. Further exposure makes the crumpled structure more noticeable with a gradual increase of t_{RMS}, 0.47 nm for $t = 100$ s and 0.57 nm for $t = 160$ s, while the overall t_H does not change appreciably. In some parts of the crumpled valleys, the peak-to-valley height begins to show a similar value to t_H of the pristine sample, indicating a local removal of graphene. These are more apparent in the sample with $t = 220$ s (figures 2(f) and 3). The graphene is completely etched away along the broadened valleys and separated clusters are formed (see the inset in figure 2(f)). t_{RMS} is measured to be 0.79 nm. The evolution of AFM images with the exposure to R-O_2 plasma reveals a microscopically homogeneous generation of crumpled structures after the first exposure, which subsequently turns into isolated graphene clusters throughout the surface. This is in comparison with what was observed in graphene oxidation where etch pits were randomly nucleated in a stochastic manner as the annealing time increases [14]. The difference can be ascribed to a strong O_2 plasma reaction to graphene, which will be discussed further.

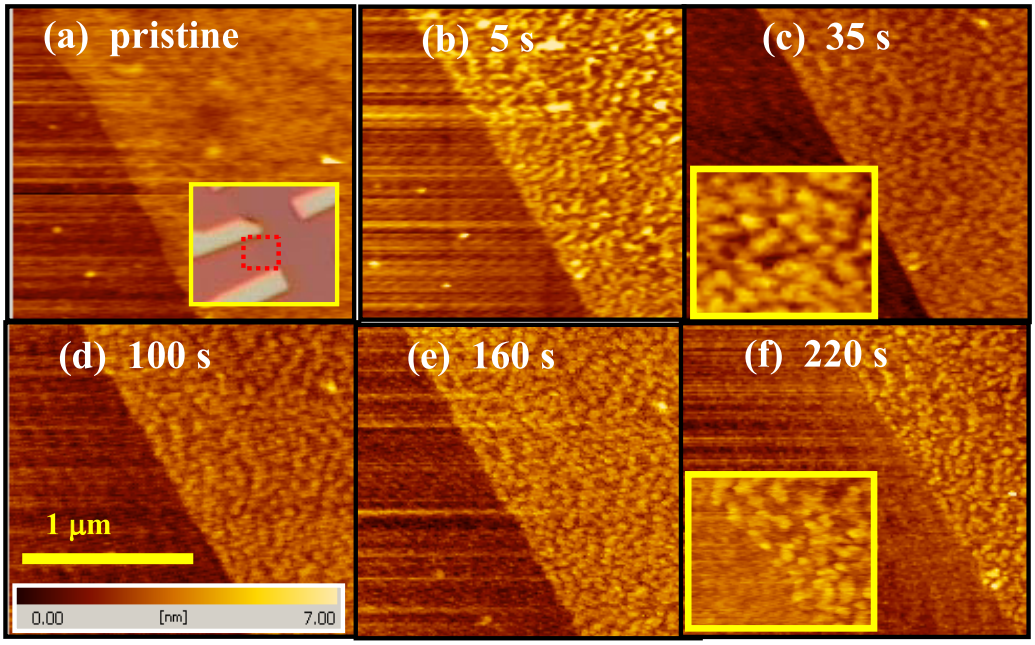

Figure 2. AFM images of a single graphene layer sample as a function of the exposure time to R-O_2 plasma. Numbers on each figure indicate the exposure time. The inset in (a) shows the microscope image of the measured sample, where the red dotted box represents the specific area where all the AFM images were taken. All figures except the insets have a size of 2×2 μm^2 with the same x–y scale and z-height scale (0–7 nm) as shown in (c). The insets in (c) and (f) have a size of 0.5×0.5 μm^2. The inset in (c) shows a typical image of the graphene surface at $t = 35$ s whereas the inset in (f) shows a typical image of graphene edges at $t = 220$ s.

Figure 4(a) shows the gate voltage (V_G) dependence of the source–drain current (I_{DS}) of the sample. The typical gate voltage dependence is observed in the pristine sample with the Dirac voltage (V_D) at ~18 V by natural hole doping [1–5]. Here the Dirac voltage is the V_G where the minimum I_{DS} is observed. The ratio of maximum to minimum I_{DS} (I_{max}/I_{min}) within the applied V_G range is 2.7. The transconductance (ϑ_m) estimated from the region of constant I_{DS}/V_G slope in the pristine sample is 1.78 nS. By exposing the pristine sample to R-O_2 plasma for just 5 s, V_D seems to shift to higher V_G, out of our measurement range. The ϑ_m decreases about an order of magnitude to 0.37 nS. The decrease of ϑ_m as well as the large positive shift of V_D is consistent with the change in electrical properties due to hole doping by oxygen plasma [16, 17]. Further increase of t leads to the decrease of I_{DS} and ϑ_m but not as drastically as shown in the first exposure case. Up to $t = 70$ s almost linear V_G–I_{DS} curves are observed without V_D. However, the sample with $t = 100$ s shows a hint of V_D with a resistance saturation at $V_G \sim 40$ V, which becomes more evident with a broad minimum of I_{DS} at $V_G \sim 0$ V for $t = 130$ s (figures 4(b) and (c)). This implies that the further exposure to oxygen plasma does not enhance the p-doping by oxygen at these stages. Still, appreciable V_G dependence can be observed with $I_{max}/I_{min} \sim 2$, comparable to 2.7 of the pristine sample (figure 5(b)). For the sample with $t = 160$ s, electrical measurements were impossible due to a high resistance of over 500 MΩ. The semi-exponential decrease of transconductance as a function of t makes us conceive of the two-dimensional percolation phenomena in graphene (figure 5(a)) [18]. The metallic conduction is only possible if the relative metallic conduction portion (P) is larger than the critical portion, the percolation threshold (P_C). The percolation theory predicts a scaling of conductance (G) as $G \propto (P - P_C)^\beta$ where β is the critical exponent. In our case, we can assume a relative portion of insulating phases ($P' = 1 - P$) to be proportional to t. If we also assume $P_C = 0.65$, that is the bond percolation threshold for a two-dimensional honeycomb lattice, and $P = P_C$ at $t = 130$ s, where the percolating metallic graphene path can still be appreciated in the V_G dependence of I_{DS} and a linear I_{DS}–V_{DS} curve (figure 4(c)), then we have $P' = \alpha t$ with $\alpha = 2.69 \times 10^{-3}$ [18]. So the scaling equation can be written as $G \propto (0.35 - \alpha t)^\beta$. The estimation of the sample conductance would be rather arbitrary due to the V_G dependence of resistance measured with a two-probe configuration. Here ϑ_m could be simply assumed to be proportional to G [17]. Then we have $\ln \vartheta_m \propto \beta \ln(0.35 - \alpha t)$, where $\alpha = 2.69 \times 10^{-3}$. The data are well fitted to the equation as shown in the inset in figure 6(a). β estimated from the constant slope is 1.23, well within the expected range of $\beta = 1.1$–1.3 for the two-dimensional percolation systems [18]. The deviation of data from the early exposure stages is easily in agreement since the scaling would not be valid in a region far from $P \sim P_C$, where the hole doping effect by oxygen plasma is also effective. The evolution of electrical properties with the exposure to R-O_2 plasma can be generally understood in terms of the percolation phenomenon. This is compatible to what was observed in the evolution of AFM images.

Figure 6 shows the evolution of Raman spectra with the exposure to R-O_2 plasma. The Raman spectra of the pristine sample, measured after the fabrication of electrodes, confirm a single graphene layer [19]. No trace of a D peak associated with disorder is observed. The standard deviation of Pos(G)

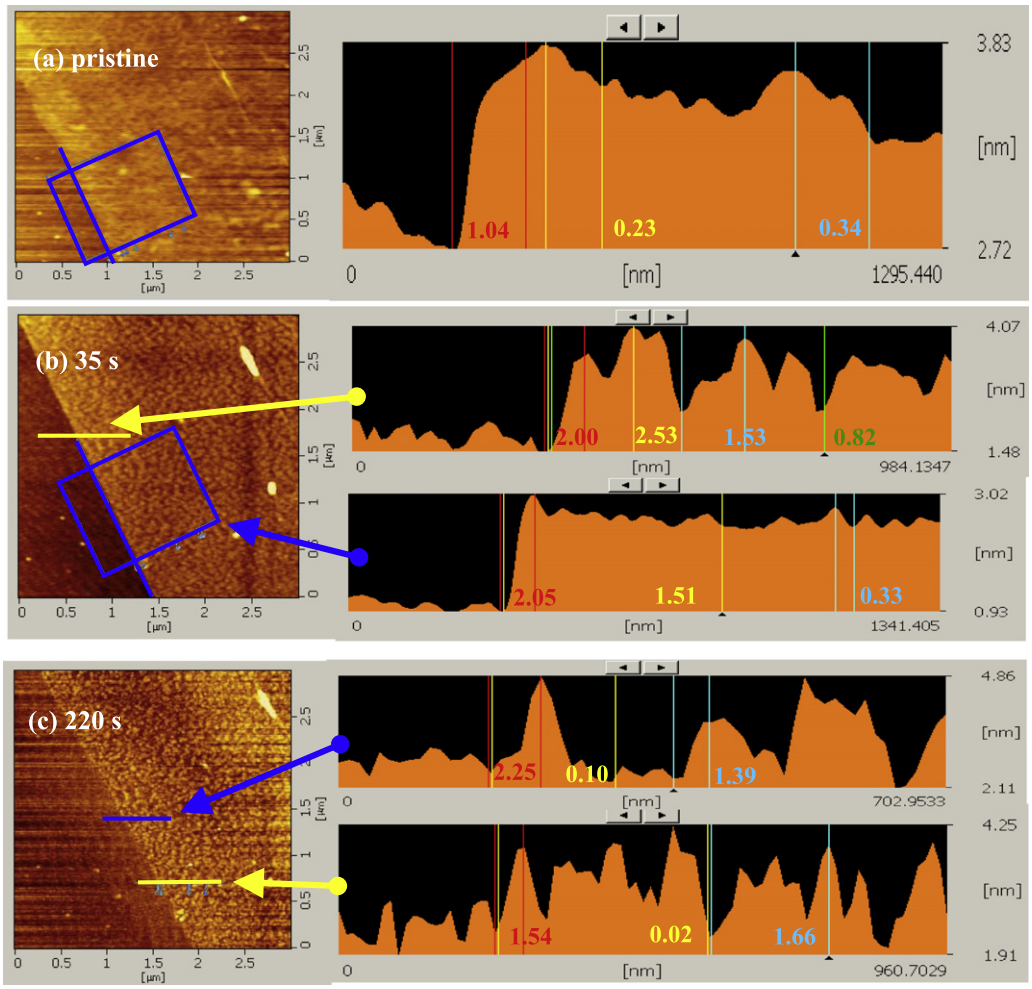

Figure 3. The height profiles of selected AFM images shown in figure 2. (a) The pristine sample shown in figure 2(a) where the right-hand image is the averaged height profile along the blue line over the surface enclosed in the blue box in the left-hand AFM image. (b) The sample with $t = 35$ s shown in figure 2(c). The upper right image is the height profile along the yellow line in the left AFM image whereas the bottom right image is the averaged height profile along the blue line over the surface enclosed in the blue box. (c) The sample with $t = 220$ s shown in figure 2(e). The right-hand images are the height profile along the lines indicated by arrows. In all the right-hand images the coloured numbers indicate the height difference (nm) of the sample between the same coloured vertical lines.

and its full width at half-maximum (FWHM) measured at four different spots in the pristine sample is not more than 1 cm^{-1}, Pos (G) $= 1581(\pm 0.7)$ cm^{-1} and FWHM $= 16(\pm 1)$ cm^{-1}, indicating good uniformity of the pristine graphene sample. The first exposure for $t = 5$ s makes the D peak appear strongly at 1341 cm^{-1} with a simultaneous appearance of the D′ peak at 1616 cm^{-1}. As t increases, the Raman spectra show systematic evolutions in peak intensity (I) and position until $t = 220$ s where no features except two small humps are observed. Here the peak intensity is defined as the peak height. It has been well known that the visible Raman spectroscopy only probes sp^2 sites by excitation of π states while amorphous carbons with sp^3 bonding generate little spectra [12, 20]. Previously a three-stage model with an amorphization trajectory ranging from graphite to amorphous carbons by disorder has been introduced, which has successfully accounted for the general features of visible Raman spectral changes in disordered graphite systems [12, 13, 20]. It would be interesting to study the disorder-induced features and their evolution of a single graphene layer in Raman spectroscopy in comparison to results from graphite systems.

The changes of Raman spectra with the exposure to R-O_2 plasma are summarized in figures 7 and 8. For the Raman peak fitting, a Lorentzian fit is used for the D, D′ and 2D peaks. The G peak is fitted with a Breit–Wigner–Fano (BWF) line, which accounts well for the residual Raman intensity at ∼1500 cm^{-1} [12, 21]. For $t = 190$ s the G and D′ peaks around 1600 cm^{-1} cannot be differentiated and are simply assumed to be a single G peak. The data obtained at $t = 220$ s are not analysed because of their low signal intensity compared to background signals. In contrast to the general features observed in the three-stage model for graphite systems by disorder, several peculiarities are found in our single graphene layer with disorder induced by oxygen plasma. Here the amount of disorder can be regarded as being proportional to t [12, 13, 20].

The first feature to note is the normalized intensity of the D mode by the G mode, $I(\mathrm{D})/I(\mathrm{G})$. It has been well

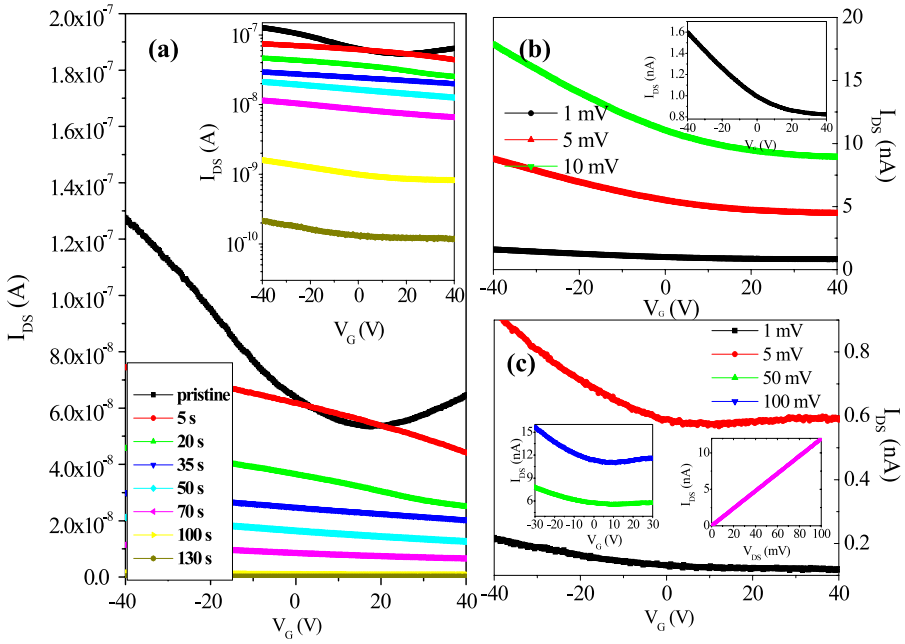

Figure 4. (a) V_G dependence of I_{DS} as a function of the exposure time to R-O_2 plasma. Here the applied V_{DS} is 1 mV. (b) V_G dependence of I_{DS} as a function of V_{DS} at $t = 100$ s. The inset shows the data with $V_{DS} = 1$ mV. (c) V_G dependence of I_{DS} as a function of V_{DS} at $t = 130$ s. The left inset shows V_G dependence of I_{DS} with $V_{DS} = 50$ and 100 mV, while the right inset shows I_{DS}–V_{DS} curve with $V_G = 0$ V. The resistance calculated from the I_{DS}–V_{DS} curve is 8.4 MΩ.

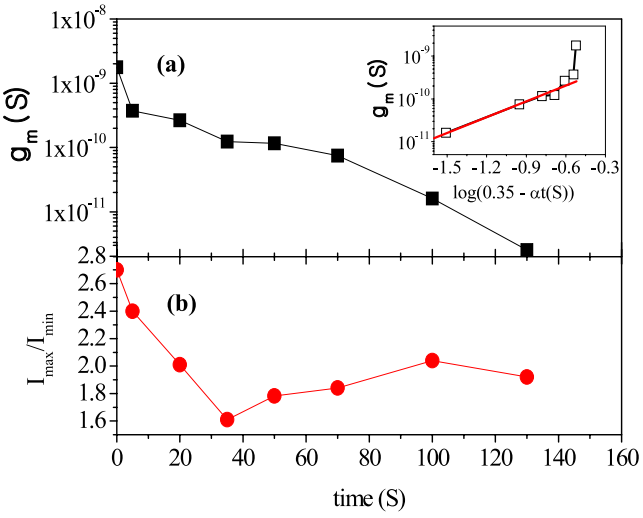

Figure 5. Exposure time dependence of (a) transconductance and (b) I_{max}/I_{min}. The inset of (a) shows the scaling behaviour of ϑ_m where the red line is a fitted curve.

established that $I(\mathrm{D})/I(\mathrm{G})$ can be used as a footprint for the amount of disorder that is directly related to the diameter of the crystalline cluster (L_a) in the graphite system. $I(\mathrm{D})/I(\mathrm{G})$ is known to be proportional to $1/L_a$ for low disorder and L_a^2 for high disorder, resulting in a broad peak-like structure in the $I(\mathrm{D})/I(\mathrm{G})$ versus L_a plot [12, 13, 20, 21]. In the experiment of R-O_2 plasma exposure, $I(\mathrm{D})/I(\mathrm{G})$ shows a sudden increase after the first exposure of 5 s up to two times and remains almost constant till $t = 50$ s, and then continues to decrease linearly with exposure time. The increase of $I(\mathrm{D})/I(\mathrm{G})$ might only exist in a very narrow window with $t < 5$ s, as revealed in the instant change of surface morphologies (figure 2(b)), compared with thermal oxygen annealing of a single graphene layer or exposure to oxygen plasma of graphene multilayers [15, 17]. This corresponds to the first stage of the three-stage model with $I(\mathrm{D})/I(\mathrm{G})$ proportional to $1/L_a$; the crystalline graphene into very fine nanocrystalline graphene grains of less than ∼2 nm [12, 13]. After $t = 50$ s, the linear decrease of $I(\mathrm{D})/I(\mathrm{G})$ can be accommodated by the second stage accompanying the decrease of $I(\mathrm{D})/I(\mathrm{G})$; from nanocrystalline graphene to amorphous carbon. The decrease of $I(\mathrm{D})/I(\mathrm{G})$ is due to the main disordering related to the decrease in the number of sp^2 ordered rings. We rule out the possibility of sp^3 bonding formation since $I(\mathrm{D})/I(\mathrm{G})$ does not go to zero and still remains ∼1 even at $t = 200$ s. Also, the FWHM of the G peak is found to be ∼60 cm^{-1} at $t = 200$ s, whereas the amorphous carbon with high sp^3 content would have 200–300 cm^{-1} [12, 20]. This implies a practical absence of stage 3 of the three-stage model involving a generation of sp^3 bonding, like in the recent Raman study of graphene with electron-beam irradiation [22]. The linear decrease of $I(\mathrm{D})/I(\mathrm{G})$ can be understood as $I(\mathrm{D})/I(\mathrm{G}) \propto L_a^2$ as expected in stage 2, consistent with the percolation analysis on our electrical measurement data [12, 13].

The second feature is that another disorder-induced mode, D′ mode, exhibits different evolutions compared to the D mode despite the fact that both D and D′ modes are activated by defects and disorder. The first exposure gives the appearance of a small D′ peak with $I(\mathrm{D}')/I(\mathrm{G}) \sim 0.36$ and a slight increase to ∼0.57 at $t = 50$ s, and then $I(\mathrm{D}')/I(\mathrm{G})$ remains rather constant (figure 7(a)) compared to the large decrease of $I(\mathrm{D})/I(\mathrm{G})$. The FWHM of the D′ peak with exposure time is also found to be inert, contrary to the increase of the FWHM of

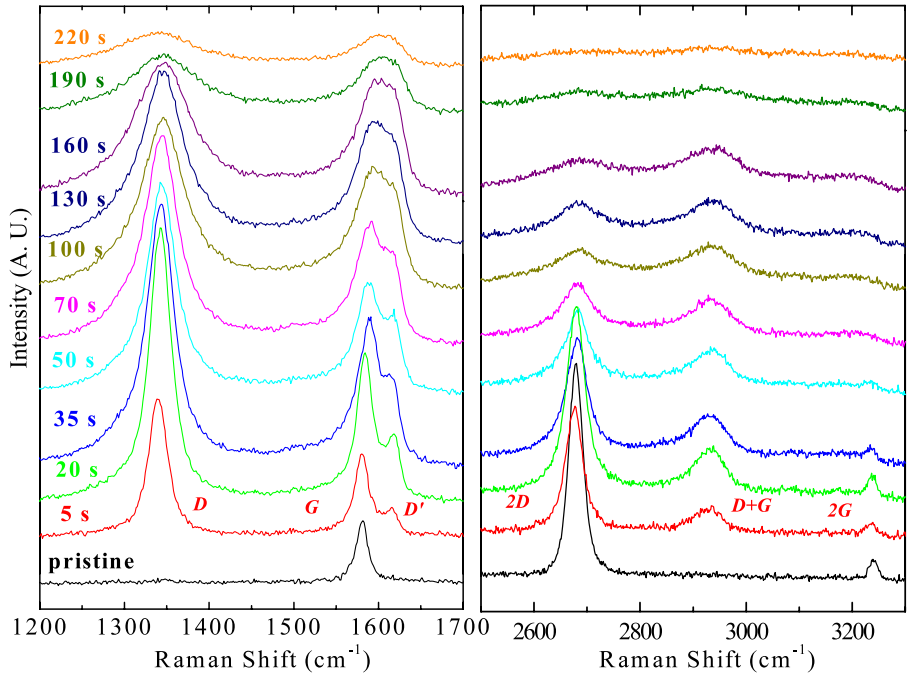

Figure 6. Raman spectra of a single graphene layer sample as a function of the exposure time to R-O_2 plasma. Numbers on the left side of the left figure indicate the exposure time. Raman peaks are indexed accordingly.

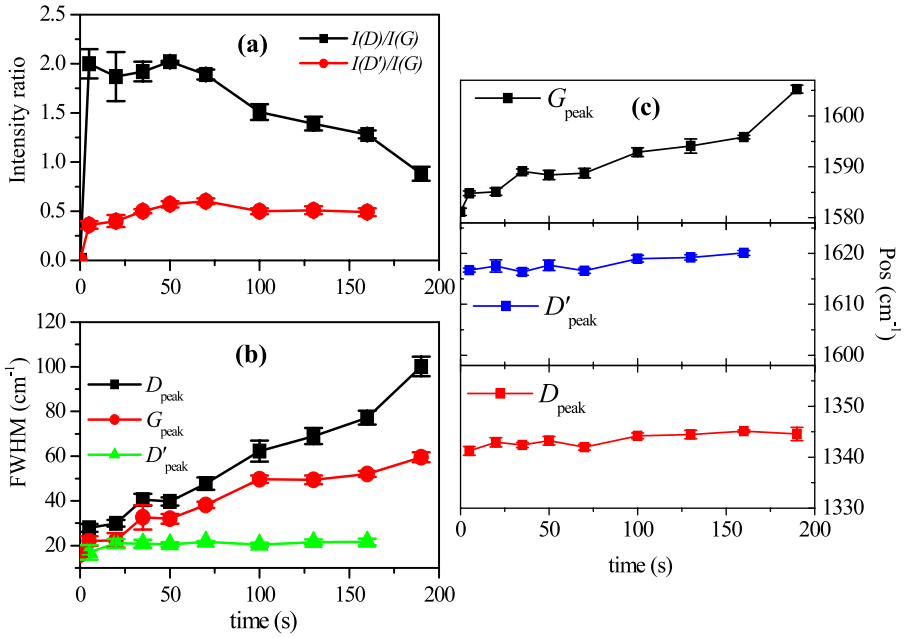

Figure 7. (a) Intensity ratio, (b) FWHM and (c) peak location of D, G and D′ modes as a function of the exposure time to R-O_2 plasma. The error bars are the standard deviation of data collected from four different spots as shown in figure 1(b).

the D peak (figure 7(b)). In fact, the disorder-induced D and D′ modes originate from different mechanisms. The former is due to the intervalley and the latter the intravalley resonant Raman mechanism [23, 24]. Only the armchair edge can contribute to the D mode by the intervalley scattering while the D′ mode is always activated independent of edge structures. Recent Raman investigation on exfoliated graphene edges reveals that I (D) does not show a significant edge orientation dependence because of microscopically disordered edge structures [25]. Similarly, since our sample is expected to have randomly arranged edge profiles of nanocrystallites with high disorder, the difference between D and D′ modes at the edges would not be so significant. It was reported that the crystallite size L_a and differential cross section affected I (D) much more than I (D′) in nanographites, which might be related to the I (D) and I (D′) difference of disordered graphene [26].

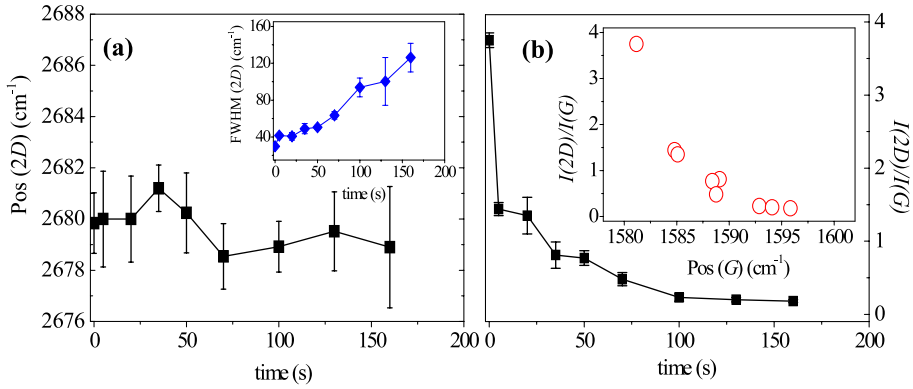

Figure 8. (a) Peak location of 2D mode and its FWHM (inset) as a function of the exposure time to R-O_2 plasma. (b) $I(2D)/I(G)$ as a function of the exposure time to R-O_2 plasma. In the inset, it is replotted as a function of Pos(G).

The last feature to be pointed out is a large shift of G peak position (Pos(G)) (figure 7(c)). The peak shift of both D and D′ modes is just about 3 cm^{-1} during the exposure. In contrast, Pos(G) increases almost linearly from 1581 cm^{-1} ($t = 0$ s) to 1596 cm^{-1} ($t = 160$ s), three times larger than that observed in the D and D′ peak shift. The initial increase of Pos(G) might be caused by an increase of defect and disorder, observable in stage 1 with low disorder [19, 27]. However, a continuous upshift of G mode in the second stage is quite different from the three-stage model of graphite, where a downshift of the G mode by disorder-induced phonon softening is observed [12, 28]. It has been reported that the G mode shows marked dependences on doping levels while the 2D exhibits negligible change and $I(2D)/I(G)$ also evolves with doping and Pos(G) [19, 29, 30]. Similar trends of $I(2D)/I(G)$ versus Pos(G) might be observed in our samples as shown in figure 8(b). This might suggest a certain role of doping by oxygen plasma on the shift of Pos(G). However, the increased FWHM of the G and the constant Pos(2D) do not seem to be explained by electrostatic doping [29, 30]. The stiffening of the G mode might be caused by localized sp^2 dimers or shorter C=C bond lengths with much higher disorder [12]. Further theoretical and experimental studies are necessary to explain the observed increase of Pos(G) in disordered single graphene layers with a decrease of $I(D)/I(G)$.

4. Summary

We report the evolution of a single graphene layer with disorder induced by R-O_2 plasma. By the first, short time exposure of about 5 s of a single graphene layer to R-O_2 plasma, a sudden change of surface morphologies is observed with the generation of a significant amount of disorder with $I(D)/I(G) \sim 2$. For t up to 50 s, while the disorder effect seems to be rather gradual as noted by almost constant $I(D)/I(G)$, the changes of electrical transport measurement data showing the V_D shift can be ascribed to the hole doping by oxygen plasma. As t increases further, the Raman data show a decrease of $I(D)/I(G)$ with a structural change from the nanocrystalline graphene phase to the sp^2 amorphous carbon phase with an increase of disorder in hexagonal carbon rings and sp^2 clustering. This change in Raman spectra can be understood in terms of a decrease of crystalline size, L_a^2, which can be directly related to the metallic conduction portion in percolation analysis of electrical measurement data. For $t > 130$ s the percolative conducting graphene paths disappear with isolated graphene clusters observable in AFM images. The evolution of AFM images, electrical transport data and Raman spectra can be well described in terms of the two-dimensional percolation theory. The Raman data show several features which were not observed before in graphite systems with disorder: a sudden appearance of a disorder-induced D mode with saturation followed by a subsequent decrease of $I(D)/I(G)$, a difference in evolution of disorder-induced D and D′ modes, and a monotonic increase of Pos (G). Our experimental data would help understand the detailed etching mechanism of graphene by oxygen plasma, which becomes important in fabrication of nanographene devices.

Acknowledgments

The authors thank Shin Keun Kim and Jehyuk Choi for helping in the operation of the remote oxygen plasma Asher, DFS-200, BMR Technology Corp., in the Korea Advanced Nanofab Center (KANC), Suwon. The authors also thank Professor G T Kim in Korea University for kindly allowing us to use an e-beam lithography machine.

References

[1] Novoselov K S, Geim A K, Morozov S V, Jiang D, Zhang Y, Dubonos S V, Grigorieva I V and Firsov A A 2004 *Science* **306** 666
[2] Novoselov K S, Geim A K, Morozov S V, Jiang D, Katsnelson M I, Grigorieva I V and Firsov A A 2005 *Nature* **438** 197
[3] Zhang Y, Tan Y-W, Stormer H L and Kim P 2005 *Nature* **438** 201
[4] Geim A K and Novoselov K S 2007 *Nat. Mater.* **6** 183
[5] Tan Y-W, Zhang Y, Bolotin K, Zhao Y, Adam S, Hwang E H, Das Sarma S, Stormer H L and Kim P 2007 *Phys. Rev. Lett.* **99** 246803
[6] Tombros N, Jozsa C, Popinciuc M, Jonkman H T and Wees B J 2007 *Nature* **448** 571

[7] Han M Y, Ozyilmaz B, Zhang Y and Kim P 2007 *Phys. Rev. Lett.* **98** 206805
[8] Ponomarenko L A, Schedin F, Katnelson M I, Yang R, Hill E W, Novoselov K S and Geim A K 2008 *Science* **320** 356
[9] Areshkin D A, Gunlycke D and White C T 2007 *Nano Lett.* **7** 204
[10] Sols F, Guinea F and Castro Neto A H 2007 *Phys. Rev. Lett.* **99** 166803
[11] Ozyilmaz B, Jarillo-Herrero P, Efetov D and Kim P 2007 *Appl. Phys. Lett.* **91** 192107
[12] Ferrari A C and Robertson J 2000 *Phys. Rev.* B **61** 14095
[13] Ferrari A C 2007 *Solid State Commun.* **143** 47
[14] Liu L, Ryu S, Tomasik M R, Stolyarova E, Jung N, Hybertsen M S, Steigerwald M L, Brus L E and Flynn G W 2008 *Nano Lett.* **8** 1965
[15] Gomez-Navarro C, Weitz R T, Bittner A M, Scolari M, Mews A, Burghard M and Kern K 2007 *Nano Lett.* **7** 3499
[16] Chen J-H, Jang C, Adam S, Fuhrer M S, Williams E D and Ishigami M 2008 *Nat. Phys.* **4** 377
[17] Kim K, Park H J, Woo B-C, Kim K J, Kim G T and Yun W S 2008 *Nano Lett.* **8** 3092
[18] Isichenko M B 1992 *Rev. Mod. Phys.* **64** 961
[19] Casiraghi C, Pisana S, Novoselov K S, Geim A K and Ferrari A C 2007 *Appl. Phys. Lett.* **91** 233108
[20] Ferrari A C and Robertson J 2001 *Phys. Rev.* B **64** 075414
[21] McCulloch D G, Prawer S and Hoffman A 1994 *Phys. Rev.* B **50** 5905
[22] Teweldebrhan D and Balandin A A 2009 *Appl. Phys. Lett.* **94** 013101
[23] Pimenta M A, Dresselhaus G, Dresselhaus M S, Cancado L G, Jorio A and Saito R 2007 *Phys. Chem. Chem. Phys.* **9** 1276
[24] Cancado L G, Pimenta M A, Neves B R A, Dantas M S S and Jorio A 2004 *Phys. Rev. Lett.* **93** 247401
[25] Casiraghi C, Hartschuh A, Qian H, Piscanec S, Georgi C, Fasoli A, Novoselov K S, Basko D M and Ferrari A C 2009 *Nano Lett.* **9** 1433
[26] Cancado L G, Jorio A and Pimenta M A 2007 *Phys. Rev.* B **76** 064304
[27] Lespade P, Marchard A, Couzi M and Cruege F 1984 *Carbon* **22** 375
[28] Beeman D, Silverman J, Lynds R and Anderson M R 1984 *Phys. Rev.* B **30** 870
[29] Yan J, Zhang Y, Kim P and Pinczuk A 2007 *Phys. Rev. Lett.* **98** 166802
[30] Das A *et al* 2008 *Nat. Nanotechnol.* **3** 210